Computationally Efficient Ship Airwake Simulations for Rotorcraft Shipboard Operations Using a GPU-Accelerated Lattice-Boltzmann Solver

Erk Kurban*
Graduate Research Assistant
Georgia Institute of Technology
Atlanta, GA 30332, USA

Shreyas Ashok
Graduate Research Assistant
Georgia Institute of Technology
Atlanta, GA 30332, USA

Juergen Rauleder
Assistant Professor
Georgia Institute of Technology
Atlanta, GA 30332, USA

ABSTRACT

It is desired to achieve computationally efficient mid-fidelity ship airwake predictions to be used in ship–rotorcraft interaction studies. The Lattice-Boltzmann Method (LBM) is a viable candidate to obtain flow field solutions rapidly, owing to its highly parallelizable nature. To demonstrate the LBM's capabilities and to show the suitability of the method to solve the large computational problem of a ship airwake simulation in a time-efficient manner, a scaled model of the SFS-2 frigate shape was simulated in uniform inflow conditions using a GPU-accelerated Lattice-Boltzmann solver. A convergence study was conducted, and it was found that the LBM results converged already at relatively coarse resolutions, but only for the mean flow quantities. The obtained results were compared to published experimental data. The LBM results showed good correlation with velocity probe measurements on the starboard side of the landing deck, but they did not predict flow asymmetry seen in the measurements. Results were also compared with particle image velocimetry data, and the flow topology as well as the mean velocity magnitudes obtained by the LBM showed excellent agreement. Satisfactory agreement was found for the turbulence intensities that were mostly underpredicted, although the gradients were correct. The LBM model was able to obtain these results in three hours and 25 minutes on eight local GPUs. Considering its computational efficiency and good accuracy for quick turn-around solutions, the current LBM model was concluded to be a good mid-fidelity alternative to high-fidelity CFD methods that require orders of magnitude more time and computational resources for ship airwake simulations.

NOMENCLATURE

ABL	Atmospheric Boundary Layer
CFD	Computational Fluid Dynamics
HPC	High-performance computing
LBM	Lattice-Boltzmann Method
LDA	Laser Doppler Anemometry
LES	Large Eddy Simulation
LHA	Landing Helicopter Assault
PIV	Particle Image Velocimetry
SFS	Simple Frigate Shape
A	Axial force effective on ship based on air loads
$A_{frontal}$	Ship frontal area facing the incoming wind, $0.06596 m^2$ for 1/50 scale model
C_A	Ship axial force coefficient based on air loads, $C_A = \frac{A}{\frac{1}{2}\rho V_\infty^2 A_{frontal}}$
C_s	Smagorinsky Constant
N_{SFS_2}	Number of computational cells along the ship length
P	Pressure
Re_L	Reynolds number based on SFS-2 model length, $\frac{U_\infty \times L_{SFS_2}}{\nu}$
SH	Ship height, 16.764 m (55 ft) for the full scale
U_∞	Uniform inflow velocity
Δ_t	Time step
Δ_x	Lattice cell edge length
$\bar{U}$	Time-averaged velocity, $\bar{u}\vec{i} + \bar{v}\vec{j} + \bar{w}\vec{k}$
$\mathbf{c_i}$	Lattice-Boltzmann discretized lattice velocity
$\overline{V_{XZ}}$	Time-averaged in-plane velocity, $\sqrt{\overline{V_X}^2 + \overline{V_Z}^2}$

Presented at the 48th European Rotorcraft Forum, Winterthur, Switzerland, September 6–8, 2022.
*Main author

$\overline{u}, \overline{v}, \overline{w}$	Time-averaged velocities in x, y, z directions
ρ	Air density
$\vec{i}, \vec{j}, \vec{k}$	Unit vectors in x, y, z directions
c_l	Lattice-Boltzmann lattice speed of sound
f_i	Lattice-Boltzmann population distributions
f_i^{eq}	Lattice-Boltzmann equilibrium population distributions
l_x, l_y, l_z	Length of the flow domain in x, y, z directions
l_{SFS2}	Length of the ship model
$u'(t), v'(t), w'(t)$	Turbulence fluctuations in x, y, z directions, $u'(t) = u(t) - \overline{u}$
$u'_{rms}, v'_{rms}, w'_{rms}$	Turbulence intensities in x, y, z directions, $u'_{rms} = \sqrt{\overline{u'(t)^2}}$
$u(t), v(t), w(t)$	Instantaneous velocities in x, y, z directions
u_l	Lattice fluid velocity
x	Streamwise direction (measured from the bow)
y	Lateral direction (measured from the ship centerplane)
z	Vertical direction (measured from landing deck surface)

INTRODUCTION

Ship deck landing is challenging even for the most experienced rotorcraft pilots. During a ship deck landing operation, the unsteady ship wake interacts with the rotor flow, necessitating continuous flight control inputs to maintain the aircraft's attitude. In order to safely and effectively train pilots to fly in such an environment, real-time piloted flight simulation is invaluable.

The SFS-2, or Simple Frigate Shape 2, is a simplified ship model created for collaborative ship airwake studies, that includes the pertinent geometry features of a frigate. The SFS-2 is obtained by adding a bow structure to the baseline SFS, and the SFS was created for collaborative studies by The Technical Cooperation Programme (TTCP) [1] as collaborative studies will save time and cost of high fidelity dynamic interface simulation development [2].

Mora [3] investigated the flow field around the SFS using oil film visualization, particle image velocimetry (PIV), and laser doppler anemometry (LDA). The results were compared with the flow field around a real frigate geometry. It was concluded that the SFS geometry results approximated the macroscopic flow field around the real frigate geometry sufficiently well.

Numerous studies have been performed on the SFS-2 airwake. Rosenfeld et al. [4] and Sydney et al. [5, 6] performed experimental studies on the SFS-2 at the Naval Surface Warfare Center, Carderock Division (NSWCCD). Effects of wind-tunnel blockage, atmospheric boundary layer simulation, and the scale of the ship model on the ship airwake were investigated by Rosenfeld et al. [4]. It was found that all geometric scales showed good agreement. The effect of the wind-tunnel blockage was found to be significant on the ship airwake, especially when considering cases with ship yaw angle. Cases with high yaw angles showed more significant wind-tunnel blockage effects. Velocity probe measurements showed that there were asymmetries in the velocity profiles with respect to the centerline of the ship under uniform inflow conditions with 0° yaw angle. Similar asymmetries were also observed in the CFD study performed by Quon et al. [7].

Sydney et al. [5] investigated the flow field around the SFS-2 using PIV measurements. This study enabled researchers to investigate the flow field not only at the landing deck but also upstream of the ship superstructure. It was observed that the upstream ship structure was responsible for a significant amount of turbulence. Moreover, the turbulence produced by the upstream ship structure was found to alter the downstream flow field. In [6] the flow field around a moving SFS-2 model was investigated by PIV, and the ship motion was found to considerably alter the flow field as compared to static ship cases.

Farish et al. [8] investigated the flow field around the SFS-2 concurrently using OpenFOAM LES, PIV, and hot-wire anemometry. In this study, high-fidelity computational results were shown to be in good agreement with experimental results. The atmospheric boundary layer (ABL) was successfully modeled using large eddy simulation (LES). In order to simulate the ABL in the wind tunnel, a Cowdrey rod grid was installed upstream of the wind tunnel test section. The same Cowdrey rod grid was modeled in the computational domain to obtain the ABL in the OpenFOAM LES simulation.

Seth et al. [9] performed PIV measurements for a scaled model of SFS-2 under uniform inflow and ABL conditions. Cowdrey rods were again used in this study to approximate an ABL inflow. The airwake was found to be unsteady and complex. Comparisons between the ship airwake under the ABL inflow and the uniform inflow were performed. These comparisons showed that most of the turbulence in the ship airwake was produced by the ship, and the turbulence effects of the ABL were secondary. Zhu et al. [10] also investigated the flow field produced by the SFS-2 model under ABL conditions. The recirculation region behind the ship superstructure was observed to have a bistable behavior. It was found that flow features and dynamics were affected

by this bistable recirculation region.

Prior work on ship airwakes is by no means limited to the SFS-2 geometry. Polsky [11] used a Navier–Stokes solver to compute the flow field around an LHA-class ship. It was found that steady-state CFD calculations were not able to obtain certain time-averaged features of the ship airwake due to its unsteady nature. Nevertheless, the airwake data obtained from this study were used in a flight simulator, and the airwake data received positive feedback from pilots in terms of providing realistic airwake effects. Another study by Polsky [12] investigated the flow field over the ships that experience beam winds using an LHA-class ship model. It was concluded that the grid quality was crucial for predicting the flow around the ship experiencing beam winds. Coarse grids were observed to predict a larger separation region compared to the actual separation region. Polsky and Bruner [13] also performed CFD analysis for the LHA-class ship, and concluded that for the LHA geometry the flow was largely Reynolds number independent. On the other hand, the flow properties were sensitive to the wind and yaw angles.

Another study with the LHA was conducted by Lee et al. [14]. In this study, CFD analysis of the LHA class ship was performed and a helicopter flight dynamics model was interfaced with CFD solutions. It was found that the unsteady ship airwake considerably changed helicopter flight characteristics and the pilot activity.

One of the most extensive reviews on ship–rotorcraft experiments and simulations was done by Shukla et al. [15]. It was noted that turbulent energy on the landing deck was primarily concentrated in the 0.2-2 Hz region and turbulent energy frequencies below 1.5 Hz on the landing deck noticeably impacted flight characteristics of the helicopter. It was claimed that coupled CFD and flight simulators were good alternatives to the wind tunnel testing for the coupled ship–rotorcraft problem. The necessity of unsteady two-way coupled simulations was also concluded by Akcengiz and Sezer–Uzol [16] due to the unsteadiness of the ship–rotorcraft problem.

This study aims to investigate the computational performance and accuracy of ship airwake simulations using a Lattice-Boltzmann Method (LBM) based flow solver. The LBM is highly parallelizable and computationally efficient. It may offer an alternative, mid-fidelity, computationally more efficient way to compute ship airwakes and rotor wakes that heavily interact during shipboard operations. Bludau et al. [17] previously used the LBM for ship–rotorcraft simulations. They used different resolutions and compared results to PIV and higher-fidelity CFD data. Bludau et al. modelled the dynamic inflow of a helicopter main rotor with LBM and validated the resulting vehicle flight dynamics [18, 19]. Horvat et al. [20] used LBM to analyze the flight path of a helicopter in an offshore wind farm. Ashok and Rauleder [21] used an Arbitrary–Lagrangian–Eulerian (ALE) moving grid formulation. Three different ALE methodologies were assessed and a newly developed method, the source term method, was found to be more favorable for rotorcraft simulations.

In this paper, the airwake of the Simple Frigate Shape 2 (SFS-2) generic ship geometry is modelled using a GPU-accelerated version of the openLB Lattice-Boltzmann solver [22], which offers a high-performance mid-fidelity alternative to conventional CFD methods. The LBM's computational speed and ability to resolve the principal physical phenomena of the flow field are assessed by an in-depth comparison of the results to experimental data. The influence of numerical simulation parameters is investigated with the goal of assessing the compromise between physical accuracy and computational performance. Based on the simulation results, the LBM's suitability for rotorcraft ship deck landing simulations is assessed.

TECHNICAL APPROACH

The Lattice-Boltzmann Method

LBM is a CFD method that models the fluid dynamics on a mesoscopic scale rather than solving the conservation of mass, momentum, and energy like other CFD methods. In the LBM, the fluid domain is represented by lattice cells in which particle distribution functions, or populations, are contained. There are a variety of lattice cell configurations that have a different number of populations. Some of the most common ones in use are D1Q3, D2Q9, D3Q15, D3Q19, and D3Q27. The naming convention of these configurations is *DkQnn*, where *k* represents the number of dimensions, i.e. the D2Q series of configurations represents the two-dimensional space. *nn* represents the number of populations in the lattice cell, i.e. D2Q9 represents a two-dimensional space and it contains nine particle populations. In this study, the D3Q19 lattice configuration was used for its computational efficiency and suitability for this current computational problem. Its particle populations are shown in Figure 1.

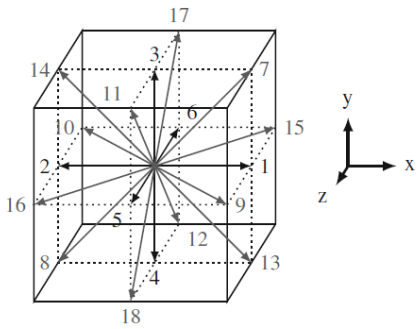

Figure 1: D3Q19 velocity set, adapted from Ref. 23.

As the simulation proceeds, populations in lattice cells are redistributed according to the Lattice-Boltzmann equation, which is given in Eq. 1.

$$f_i(\mathbf{x}+\mathbf{c_i}\Delta t, t+\Delta t) = f_i(\mathbf{x},t) - \frac{\Delta t}{\tau}(f_i(\mathbf{x},t) - f_i^{eq}) \quad (1)$$

Eq. 1 was derived from the discretized Boltzmann equation. The last term on the right hand side, $-\frac{1}{\tau}(f_i(\mathbf{x},t)-f_i^{eq})$ is known as Bhatnagar-Gross-Krook (BGK) collision operation, [24]. The BGK dynamics model relaxes populations to the equilibrium state, f_i^{eq}. This relaxation is done at a rate that is determined by τ, the relaxation time. The equilibrium state is given by Eq. 2.

$$f_i^{eq}(\mathbf{x},t) = w_i\rho\left(1+\frac{\mathbf{u_l}\cdot\mathbf{c_i}}{c_l^2}+\frac{(\mathbf{u_l}\cdot\mathbf{c_i})^2}{2c_l^4}-\frac{\mathbf{u_l}\cdot\mathbf{u_l}}{2c_l^2}\right) \tag{2}$$

In Eq. 2, w_i is the specific weight of the population i, ρ is the lattice density, $\mathbf{u_l}$ is the lattice fluid velocity, $\mathbf{c_i}$ is the discretized lattice velocity, and c_l is the lattice speed of sound. With c_l, pressure and density can be related in terms of lattice units as in Eq. 3.

$$P = c_l^2\rho \tag{3}$$

c_l can be obtained by Eq. 4, where Δx is the lattice cell edge length, and Δt is the time step.

$$c_l^2 = \frac{1}{3}\frac{\Delta x^2}{\Delta t^2} \tag{4}$$

In Eqs. 5 and 6, expressions for the lattice density and momentum are shown.

$$\rho(\mathbf{x},t) = \sum_i f_i(\mathbf{x},t) \tag{5}$$

$$\rho\mathbf{u_l}(\mathbf{x},t) = \sum_i \mathbf{c}_i f_i(\mathbf{x},t) \tag{6}$$

The lattice density given in Eq. 5 and the lattice momentum given in Eq. 6 are in terms of lattice units. These can be converted to physical units (kg/m^3, kg m/s) with the use of a simple physical conversion factor.

Simulation Parameters

For this study, the LBM simulation was set up to produce the flow conditions tested in Rosenfeld et al. [4] for the experimental test case with a uniform inflow condition of $V_\infty = 15.433$ m/s and a 1:50 scale SFS-2 model. The model length was 2.774 m, and the Reynolds number based on ship length, Re_L, was 2.9×10^6. Comparison point velocity results were collected at eight points above the landing deck. These results were compared to data obtained by Rosenfeld et al. [4] from eight fast-response velocity probes placed at the same locations.

The velocity probe locations are tabulated in Table 1. The coordinate system origin was located at the bow of the ship. Measurements were taken up to a height of 0.5 m above the deck surface. The axes and origin are shown in Figure 2. It should be noted that these probe locations were used by Rosenfeld only for the 0° yaw at 1:50 scale. The data

Table 1: Probe locations for 1:50 scale model 0° yaw case

Probe	x [in]	y [in]
A	100	-4.5
B	100	-1.5
C	100	1.5
D	100	4.5
E	109.2	-4.5
F	109.2	-1.5
G	109.2	1.5
H	109.2	4.5

provided by Rosenfeld et al. [4] also includes 1:100 scale cases, which use different probe locations.

A Smagorinsky turbulence model was used with a Smagorinsky constant of 0.05. In large eddy simulations, turbulence scales which are smaller than the grid resolution are not resolved. To model the effect of these sub-grid turbulence scales, an eddy viscosity is specified, which introduces additional dissipation. In the Smagorinsky turbulence model, the eddy viscosity is determined based on the stress tensor, which was formulated by Pope [25] as Eq. 7.

$$\nu_{sgs} = (C_s\Delta_x)^2\sqrt{2S_{ij}S_{ij}} \tag{7}$$

Δ_x is the mesh size, S_{ij} is the strain rate tensor, and the coefficient C_s is the Smagorinsky constant. A key advantage of the Smagorinsky model in the LBM framework is that the stress tensor S_{ij} can be calculated locally for each cell, which yields highly-efficient parallelization.

A convergence study was conducted to choose the simulation time period or simulated time. The axial force on the ship was computed and its convergence was assessed. Based on the force results, it was determined that the simulation was converged after 1.5 s of simulated time, and all initial transients had dissipated. Therefore, a total simulation time of 3 s was selected, during which 1000 flow realizations were saved from $t = 2$ s to $t = 3$ s to determine time-averaged quantities. Another convergence study was conducted to choose the resolution. The number of computational cells along the ship length, N_{SFS_2}, was varied and convergence was obtained for $N_{SFS_2} = 700$, resulting in a cell edge length of 3.963 mm and total cell count of 2.058×10^9 grid cells in the computational domain (see Fig. 3). Furthermore, turbulence quantities were monitored and compared to measurements, to give another measure for convergence in addition to the averaged velocities and integrated axial force. Results from the convergence studies are shown in the subsequent section.

The fluid domain had the dimensions of $l_x = 4\times l_{SFS2}$, $l_y = 1.5\times l_{SFS2}$, and $l_z = l_{SFS2}$, where l_{SFS2} was the length of the ship model. A schematic of the simulation domain is shown in Figure 3 and the time step was $\Delta t = 1.72\times10^{-5}s$. A convergence study for the time step was also conducted, but is not shown for brevity. This convergence study suggested that decreasing Δt further did not lead to significant

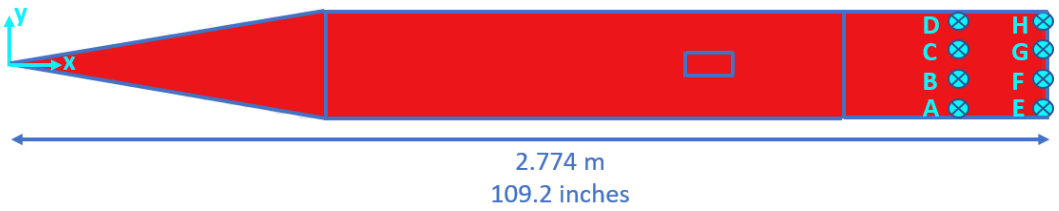

Figure 2: Coordinate axes on the 1:50 scale ship model and velocity probe locations A-H.

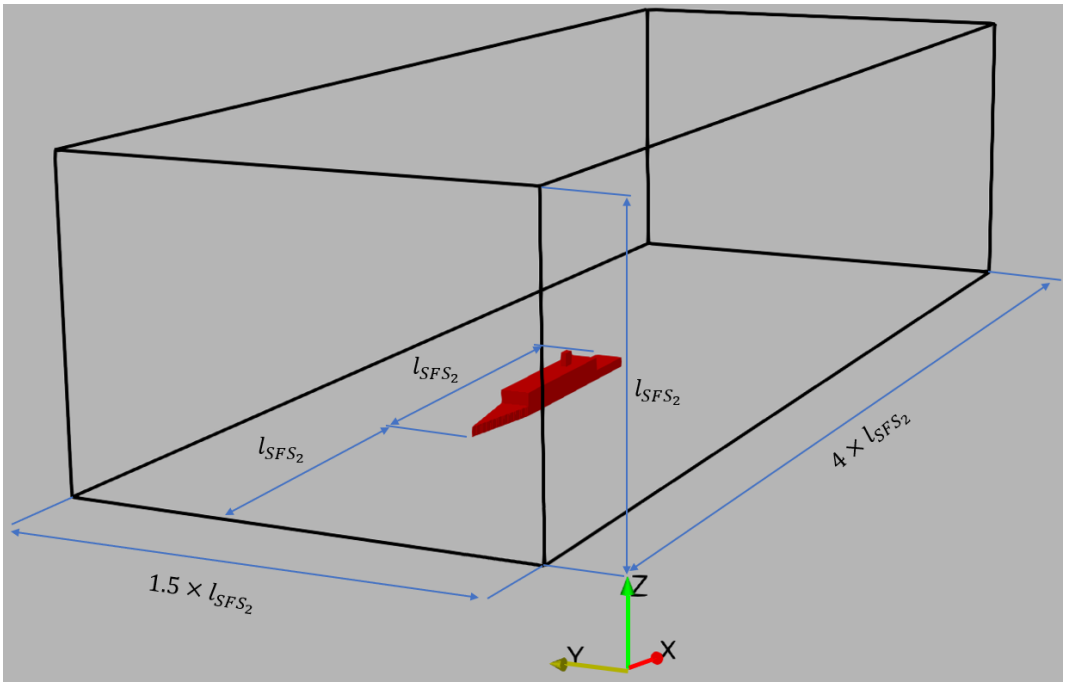

Figure 3: Computational domain used for the LBM simulations.

changes in the results. The current LBM simulations used eight local NVIDIA A100 80GB GPUs in parallel, and the final simulation configuration used 26.8 GB of GPU memory per graphics card.

For the final simulation configuration, the simulation runtime was three hours and 25 minutes on these eight GPUs, which is orders of magnitude lower than the computational expense of more conventional URANS based computations. For example, LES simulations were reported in Ref. 8, and the runtime of those simulations was in the order of weeks on a high-performance computing (HPC) cluster for the same computational problem. Computationally more efficient simulations reported in Ref. 7 used 128 processors on an IBM iDataPlex platform and were obtained in 4.2, 16.7 and 10.4 hours for 1000 iterations for URANS simulations of the wind tunnel test section, URANS simulations in free air, and hybrid free-air simulations, respectively. The hybrid approach used URANS for the near-body solution coupled with wake modeling methodologies. In this case, VorTran-M, an Eulerian vorticity transport solver was used for the wake and combined with FUN3D (URANS) for the near-body solution. VorTran-M used in Ref. 7 was the serial version, and further speed-up was expected when using the parallelized version of VorTran-M.

At the inlet, an equilibrium boundary condition was used to apply a uniform velocity profile. The equilibrium boundary condition prescribed all of the Lattice-Boltzmann populations at the inlet cells to the equilibrium state corresponding to the freestream velocity of $V_\infty = 15.433$ m/s. This boundary condition was justified because the inlet was sufficiently far from the ship model, and any deviations from the equilibrium at the inlet were found to be negligible. Slip boundary conditions were applied to the top, bottom (i.e., the water surface), port, and starboard boundaries of the domain. A bounce-back boundary condition, which models a no-slip wall, was applied to the ship surface. At the outlet, a pressure boundary condition was used which enforces $\frac{\partial p}{\partial n} = 0$.

RESULTS AND DISCUSSION

Convergence Study for Smagorinsky Constant, Simulation Time, and Resolution

In this section, a parametric study of simulation parameters is discussed. A parametric study varying the Smagorin-

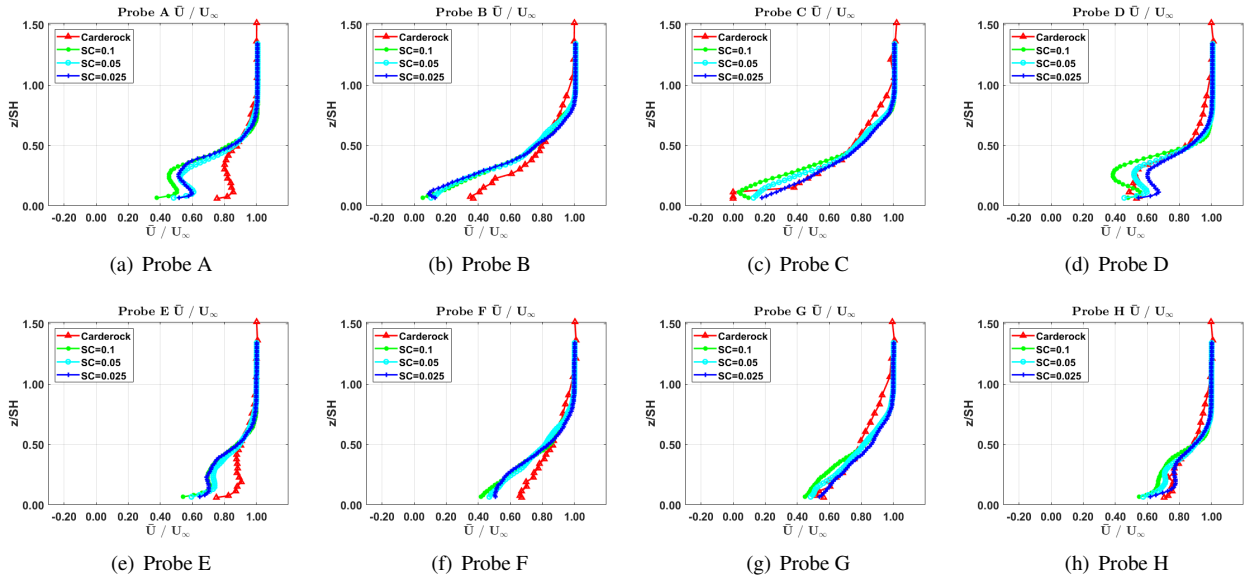

(a) Probe A (b) Probe B (c) Probe C (d) Probe D

(e) Probe E (f) Probe F (g) Probe G (h) Probe H

Figure 4: Average velocity magnitudes normalized by freestream velocity for probes A-H obtained by Rosenfeld (Carderock) [4] for 1:50 scale ship model, LBM simulation with $C_s = 0.1$, $C_s = 0.05$, and $C_s = 0.025$ for 1:50 scale ship model. z is the distance measured from landing deck surface normalized by ship model height (SH=0.335 m), positive up.

sky constant, and resolution was conducted to determine the optimum simulation configuration for this problem that provided high computational performance without compromising the accuracy of the results. The total simulation time was decided by convergence of airloads effective on the ship. The computational results were compared with the velocity probe data of Rosenfeld et al. [4].

Smagorinsky Constant Bludau et al. [17] used $C_s = 0.025$ for the full-scale ship with $Re_L = 142 \times 10^6$. However, the experimental results of Rosenfeld et al. [4] were obtained for a 1:50 scale model of the ship with $Re_L = 2.9 \times 10^6$. The stark difference in Reynolds number might affect the turbulence behavior and alter flow features. Hence, the effect of the Smagorinsky constant should be investigated. Smagorinsky constants of 0.025, 0.05, and 0.1 were evaluated.

The data set of Rosenfeld et al. [4] contains velocity magnitude averages for eight probes. The results obtained using LBM were compared to the data of Rosenfeld et al. [4]. Turbulence measurements for these tests were not available. As a result, only averaged velocity quantities can be compared. In Figure 4, a comparison between the data obtained from LBM and data of Rosenfeld et al. [4] was shown for average velocity magnitudes normalized by freestream velocity at all probe locations for different Smagorinsky constants.

It can be seen clearly in Figure 4 that apart from the near-body regions of Probe A, B, E, and F, the LBM results correlated well with the experimental data. At higher z, away from the ship body, the Smagorinsky constant did not affect the flow, while near the ship deck, a Smagorinsky constant of $C_s = 0.05$ showed the best agreement with the experimental data.

The LBM results agreed very well on the starboard side, but the correlation of the LBM results on the port side was not as good, especially in regions closer to the landing deck. It should be noted that probes A and D, B and C, E and H, and F and G were symmetrical with respect to the centerplane of the ship model. One would expect probe data to be symmetric for symmetrical probe locations, but it was shown that [4] there was asymmetry in the flow over the landing deck. This asymmetry was not reflected in the LBM results.

Simulation Time The simulation time should be as small as possible to save computational resources. On the other hand, the flow solution must be adequately converged and represent the pertinent time scales of the flow physical problem of interest. Note that the results presented in the previous subsection were obtained from 5-second simulations, and 1000 flow realizations were obtained during the last second (t=4 s to t=5 s) for averaging.

To check convergence, the axial force on the ship was computed using the momentum-exchange approach [22, 26]. It was assumed that if the ship axial force from the airloads alone was converged, the ship airwake was converged and the flow was free of significant transients. As shown in Figure 5, the difference between the axial force coefficient and the converged axial force coefficient was reduced to below 10% after t=1.5 s. Considering a deviation of 10% to be satisfactory (given that the objective of this current mid-fidelity modeling approach is a good compromise between

accuracy and computational expense) the ship airwake solution was considered converged after t=1.5 s.

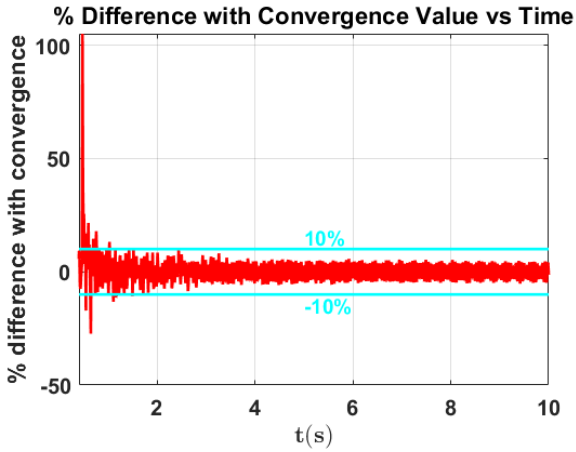

Figure 5: Axial force coefficient over time.

As can be seen in Figure 6, the axial force coefficient at convergence was 0.598. This corresponds to the drag force on the ship resulting from the airloads and not considering any ship structure below the waterline. Blount and Bartee [27] stated that for head-wind conditions, the drag coefficient (based on airloads) for most ship geometries was between 0.5 and 0.8. Considering their findings, $C_A = 0.598$ was a reasonable estimate. However, it is important to note that this current study was intended to be a mid-fidelity approach for good/quick estimates and quick turn-around solutions and, therefore, the grid resolution was relatively coarse for an accurate near-body solution.

The coarse resolution led to two side effects. Firstly, this coarse resolution was not expected to resolve the turbulent ship boundary layers. Secondly, because of the representation of the ship with the bounce-back boundary condition, the actual ship surface was represented as a voxelized solid, which can be sufficient for flow field studies but is not necessarily adequate for accurate force measurements. Therefore, it was not expected that the computed ship airloads or

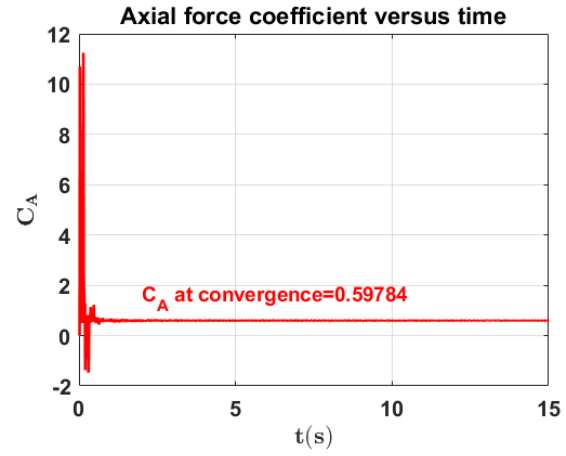

Figure 6: Axial force coefficient over time.

axial force results were fully accurate, and they were primarily obtained for the intent of determining convergence.

Based on this convergence study, it was determined that any instantaneous flow realizations should be saved after t=2 s of simulation time to ensure that the initial transients had dissipated. For ensemble averaging, 1000 flow realizations were obtained from t=2 s to t=3 s.

Resolution Thus far, all presented results used a resolution of $N_{SFS_2} = 780$ computational cells per ship length. However, it is possible that reducing the resolution might preserve acceptable physical accuracy while saving computational time. To investigate this, simulations with $N_{SFS_2} = 700$, $N_{SFS_2} = 600$, $N_{SFS_2} = 500$, $N_{SFS_2} = 400$, $N_{SFS_2} = 300$, $N_{SFS_2} = 200$, and $N_{SFS_2} = 100$ were tested.

Previously, it was shown that the port side probe velocity measurements given [4] were not symmetrical with the starboard side probe measurements. The LBM results correlated well with the measurements of Rosenfeld et al. [4] on the starboard side of the landing deck, where probes C, D, G, and H were located. So far, results from both the port side and the starboard side were presented, but for the resolution studies, only the starboard data are shown.

From Figure 7 it can be seen that simulations with $N_{SFS_2} = 100$, $N_{SFS_2} = 200$, and $N_{SFS_2} = 300$ were not grid-independent. It should be noted that the near-body velocity was smaller in magnitude for these coarse resolution cases. This indicated that separation regions obtained for a coarse resolution were larger than the ones obtained for the higher resolution simulations. Polsky [12] also observed larger separation regions for coarse resolutions.

Convergent behavior was found with increasing the resolution, and the simulation with $N_{SFS_2} = 700$ was chosen as a good compromise between computational time and accuracy, as it produced almost the same result as the simulation with $N_{SFS_2} = 780$, but with significantly fewer grid cells. Note that all of the LBM simulations used Cartesian meshes with uniform cell sizes and, therefore, a small reduction in cell numbers along the ship has a large impact on the overall cell count in the domain and hence the computational time. The number of total grid cells in the domain with $N_{SFS_2} = 780$ was 2.847312×10^9, while the number of grid cells using $N_{SFS_2} = 700$ was 2.058×10^9. Therefore, the total number of grid cells was decreased by over 27% without significant variance in the results for the averaged quantities and turbulence quantities. One can argue that $N_{SFS_2} = 600$ gave accurate results as well, according to Figure 7. However, convergence of averaged quantities was not adequate to claim grid independence. When the turbulence quantities were examined, the simulation with $N_{SFS_2} = 600$ was found to significantly underpredict the turbulence quantities. Hence, $N_{SFS_2} = 700$ was deemed the minimum viable resolution to obtain accurate turbulence quantities.

The final configuration for the simulation had $N_{SFS_2} = 700$ cells, with a cell edge length of 3.963 mm. The simula-

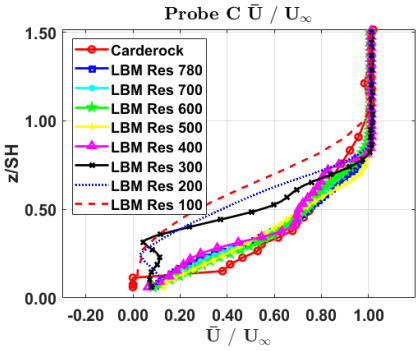

(a) Probe C

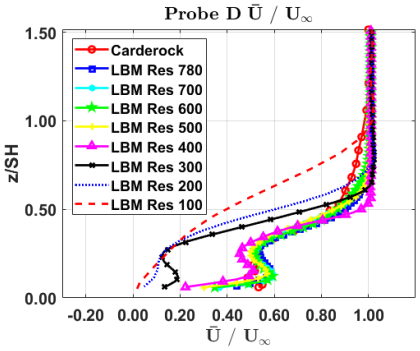

(b) Probe D

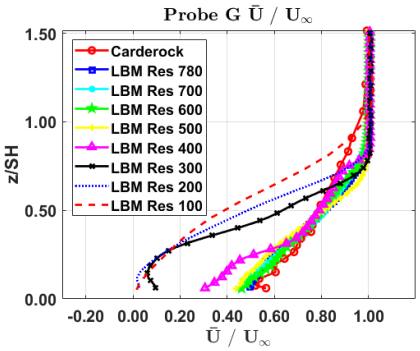

(c) Probe G

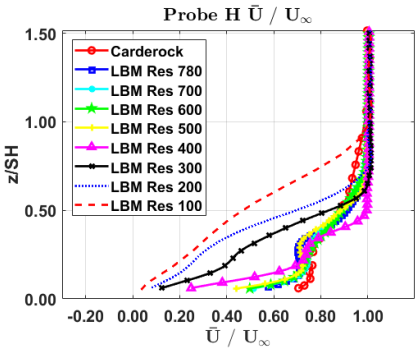

(d) Probe H

Figure 7: Average velocity magnitudes normalized by freestream velocity obtained from LBM simulations for different resolutions compared to measurements [4] for 1:50 scale ship model at probes C, D, G, and H, which are located on the starboard side of the landing deck

tion duration was three seconds, and 1000 flow realizations were used from t=2 s to t=3 s for the averaged quantities. A Smagorinsky constant of $C_s = 0.05$ was used. The simulation runtime was three hours and 25 minutes. Therefore, the LBM provided results orders of magnitudes faster than conventional URANS based solvers. For example, Farish et al. [8] conducted LES simulations, and the runtime of their simulations was in the order of weeks. Depending on the objectives of the flow field computations, if the user is willing to trade some accuracy with computational expense, lower resolution cases were still giving acceptable agreement with the measurements. For $N_{SFS_2} = 600$ the simulation runtime was one hour and 50 minutes, and for $N_{SFS_2} = 400$ it was less than 50 minutes.

Final Simulation Configuration Compared with Velocity Probe Data

The results from the final simulation configuration discussed previously were then compared in depth to the data of Rosenfeld et al. [4]. The experimental results also include data for the 1:100 scale ship model tested in uniform inflow with 30.86 m/s, which corresponded to $Re_L = 2.9 \times 10^6$. The Reynolds numbers were the same for the 1:50 scale Carderock case, the 1:100 scale Carderock case, and the LBM case.

In Figure 8, it can be seen that the LBM results correlated very well with the measurement data from Rosenfeld et al. [4] on the starboard side, where probes C, D, G, and H were located. The probe data for the 1:100 scale ship model deviated from the simulations and probe data for the 1:50 scale ship model at probe D. However, this deviation only occurred in a region closer to the landing deck (z/SH <0.3). All probe results on the starboard side correlated well for higher elevations above the deck. On the port side, where probes A, B, E, and F were located, the results did not agree as well [4] due to the aforementioned asymmetry with respect to the starboard probes. It was seen [4] that the asymmetry was less significant closer to the centerplane. Indeed, it was observed in the present study that the lack of symmetry of the LBM results was less significant for probes B, C, F, and G, which were closer to the centerplane than the other probes.

Quon et al. [7] observed asymmetry in probe data for a similar case. Their study used high-fidelity URANS and hybrid solvers, and unsteady shedding from the side walls of the ship structure was observed. Quon et al. [7] called the interactions with unsteady shedding "chaotic." Farish et al. [8] also observed noticeable differences between the data sets for probes A and D. They concluded that even small differences in sample locations lead to significant differences in measured flow quantities.

The reason behind the sensitivity can be explained by the location of probes A and D. In Figure 9, the average velocity is shown on a horizontal plane located 0.1 m above the landing deck. It can be seen that probes A and D were in

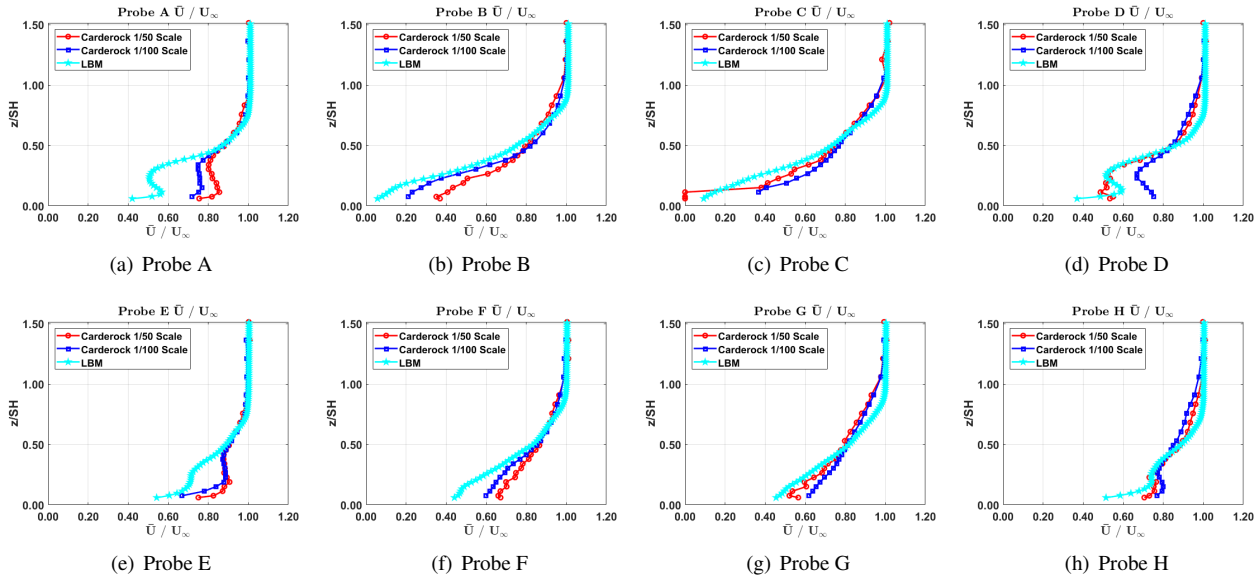

(a) Probe A (b) Probe B (c) Probe C (d) Probe D

(e) Probe E (f) Probe F (g) Probe G (h) Probe H

Figure 8: Average velocity magnitudes normalized by freestream velocity for probes A-H obtained by Rosenfeld (Carderock) [4] for 1:100 scale ship model and 1:50 scale ship model, LBM simulation with $N_{SFS_2} = 700$ resolution for 1:50 scale ship model. z/SH is the distance measured from landing deck surface normalized by ship height (SH=0.335 m for 1:50 scale, SH=0.168 m for 1:100 scale), positive up.

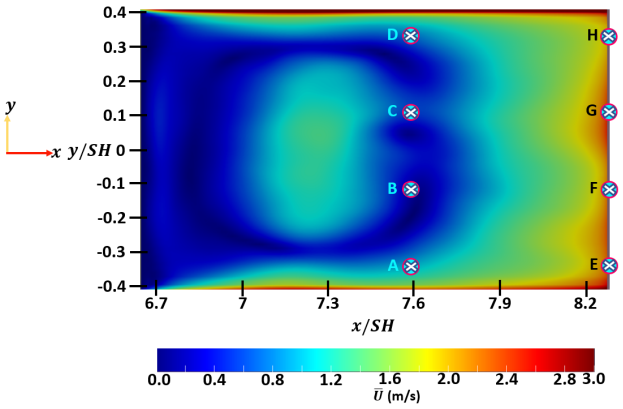

Figure 9: Time-averaged velocity magnitude 0.1 m over the landing deck with probe locations shown.

the vicinity of a shear layer, where the flow gradients were intense. As a result, a slight variation of the probe locations A and D can yield significantly different measurements. This is made further evident by extracting velocity values at slightly shifted probe locations. In Figure 10, results are plotted for probe A at its original location, as well as for two locations which were obtained by shifting the probe by 10 and 20 mm towards the port side, respectively. Clearly, as the probe was shifted towards the port side, the LBM results agreed better with the Carderock measurements.

It is likely that due to the mid-fidelity nature of the current study and relatively coarse grid resolutions, the LBM could not exactly obtain the location of the shear layer near probe A, because small unsteady structures that may have induced the strong asymmetries were not resolved. More significant unsteady shedding and, consequently asymmetry, might have been obtained using curved slip-wall boundary treatments applied by Fernandez et al. [28], but this would need further investigation. Apart from the near-landing deck region on the port side, the LBM predicted the flow field very well. A closer look at the flow fields on the landing deck is provided in the following section.

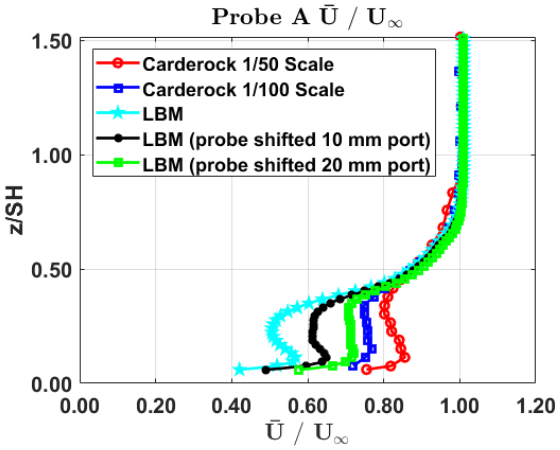

Figure 10: Average velocity magnitudes normalized by freestream velocity at probe A, probe location shifted 10 mm port side of probe A, and probe location shfited 20 mm port side of probe A, obtained by LBM simulation with $N_{SFS_2} = 700$ resolution for 1:50 scale ship model compared with experimental probe data by Rosenfeld (Carderock) [4]. z/SH is the distance measured from landing deck surface normalized by ship height (SH=0.335 m for 1:50 scale, SH=0.168 m for 1:100 scale), positive up.

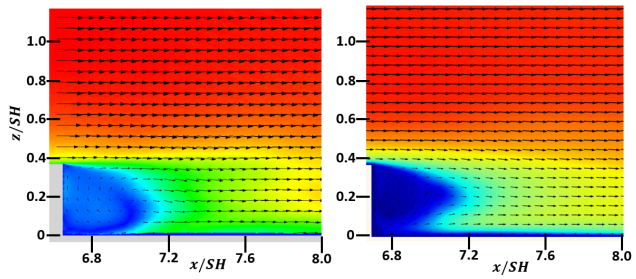

(a) Plane A

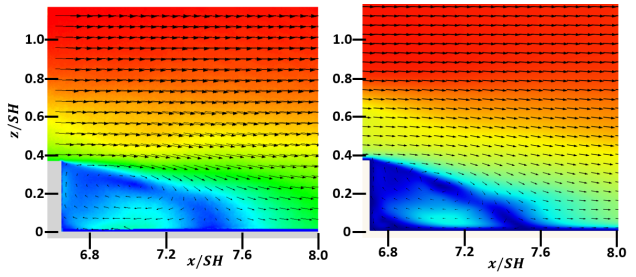

(b) Plane B

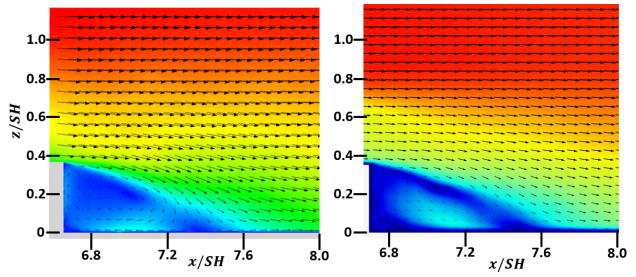

(c) Plane C

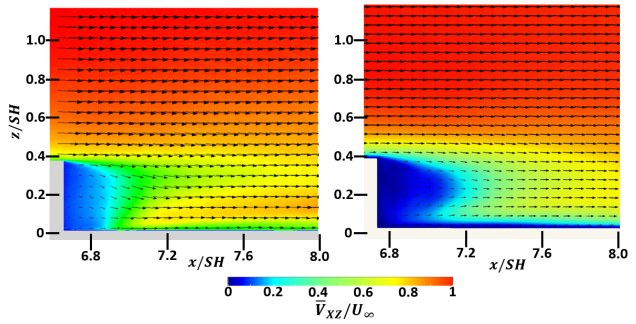

(d) Plane D

Figure 11: Time-averaged in-plane velocity magnitudes normalized by freestream velocity, $\overline{V_{xz}}/U_\infty$, from PIV results provided by Rosenfeld et al. [4] on left and results of LBM on right for the planes where probes A, B, C, and D are located, both for $Re_L = 2.9 \times 10^6$ under uniform inflow conditions.

Flow Field Comparisons

Flow field results from the final configuration of the LBM simulation were compared to the available data. Rosenfeld et al. [4] provided time-averaged in-plane velocity normalized by the inflow velocity, $\overline{V_{XZ}}/V_\infty$ obtained by PIV at planes where probe A, B, C, and D were located for the 1:100 scale model. Because the Reynolds number of the 1:100 scale cases was $Re_L = 2.9 \times 10^6$, these results were directly comparable to those from the present LBM computations.

Minor asymmetries were observed [4] in the PIV results, similar to the ones shown in the velocity probe data. Recall that planes A and D were located symmetrically with respect to the center plane of the ship, and planes B and C were also located symmetrically with respect to the center plane of the ship. In the PIV results [4], which can be seen on the left-hand side of Figure 11, one can see the asymmetry between plane A and plane D. LBM results matched excellently with PIV results for plane A, plane B and plane C. The LBM results were symmetric for planes A and D. For the PIV results of Rosenfeld et al. [4], plane D had a slightly shorter separation region, which was adjacent to the hangar. LBM did not obtain the small separation region obtained by PIV at plane D. Rather, it obtained a separation region more like the one in plane A. Still, plane D results obtained by the LBM showed acceptable agreement.

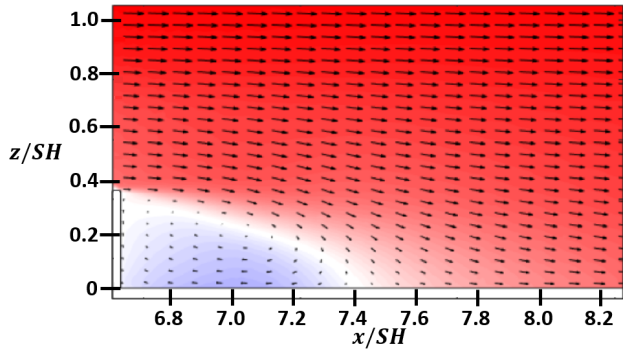

(a) PIV [9]

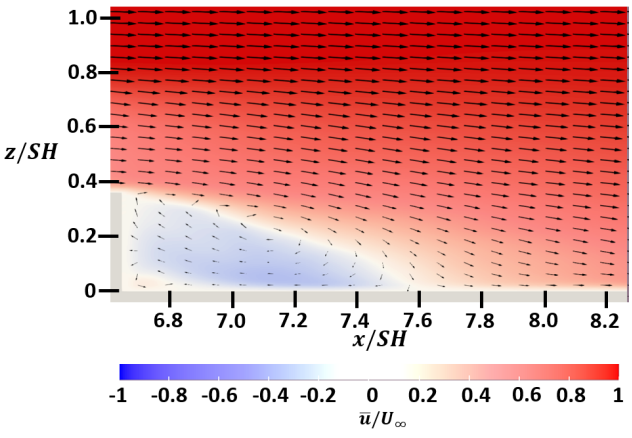

(b) LBM

Figure 12: Time-averaged streamwise velocity normalized by freestream velocity, $\overline{u}/U_\infty$, obtained from PIV [9] for $Re_L = 3.1 \times 10^6$, and from LBM for $Re_L = 2.9 \times 10^6$, both for uniform inflow conditions at the centerplane of the landing deck.

In Seth et al. [9], time-averaged streamwise velocities and

time-averaged vertical velocities were provided at the center plane of the landing deck for a Reynolds number of $Re_L = 3.1 \times 10^6$ under uniform inflow conditions. The difference between the Reynolds number for the case run in LBM ($Re_L = 2.9 \times 10^6$) and PIV data provided [9] was small, and so the results were deemed comparable. In Figure 12, it can be seen that the LBM results and PIV results of Seth et al. [9] were very similar. The recirculation regions showed good agreement between the LBM results and PIV data, and the overall flow topology correlated well with the PIV results [9].

It is important to correctly predict vertical flow velocity gradients behind the hangar, as these gradients directly impact rotor thrust for rotorcraft operating near this region. These gradients were visualized by averaging the vertical velocity. In Figure 13, the time-averaged vertical velocity was compared with the PIV results [9].

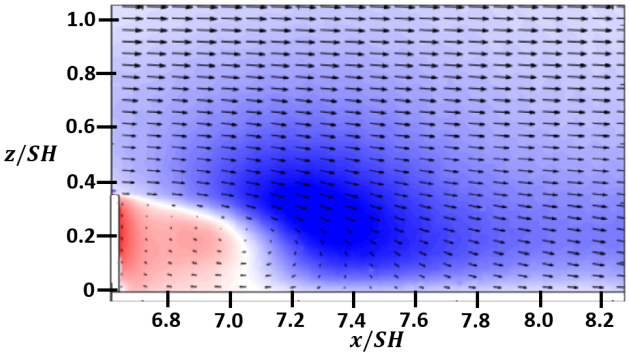

(a) PIV [9]

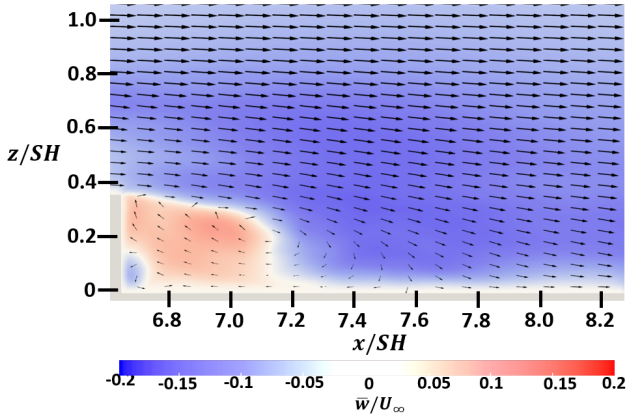

(b) LBM

Figure 13: Time-averaged vertical velocity normalized by freestream velocity, $\overline{w}/U_\infty$, obtained from PIV [9] for $Re_L = 3.1 \times 10^6$, and from LBM for $Re_L = 2.9 \times 10^6$, both for uniform inflow conditions at the centerplane of the landing deck.

In Figure 13, it can be seen that the result obtained by LBM resembled the PIV results [9]. However, it was quite interesting that the recirculation region obtained by LBM enclosed a small region (Figure 13, blue region inside red region) where the flow convected toward the landing deck (ground). This was not observed [9] in the PIV measurements. In the context of a helicopter landing approach, this discrepancy would not pose a problem, as the main rotors of the aircraft do not significantly interact with the small region at the corner of the landing deck and the hangar. Apart from this minor difference, the size of the recirculation region was found to be almost identical to the PIV results.

Thus far, the centerplane time-averaged PIV data of Seth et al. [9] showed that the LBM predicted the flow topology well. However, obtaining time-averaged quantities is not enough to show that LBM would be a suitable method for being used in ship–rotorcraft interaction simulations. Turbulence quantities also need to be correctly predicted for this application because the interaction of the ship airwake turbulence with helicopter rotors is one of the fundamental reasons why ship deck landing is so challenging. Consequently, turbulence quantities also need to be investigated to prove the capabilities of LBM.

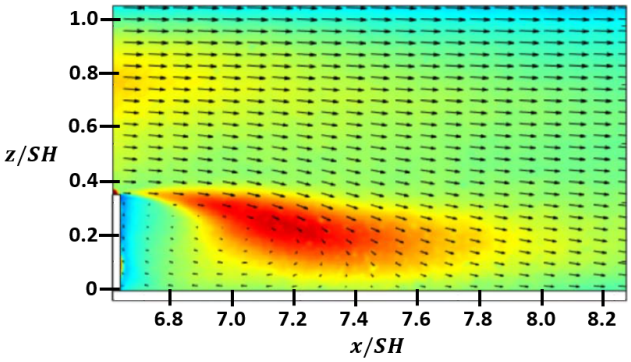

(a) PIV [9]

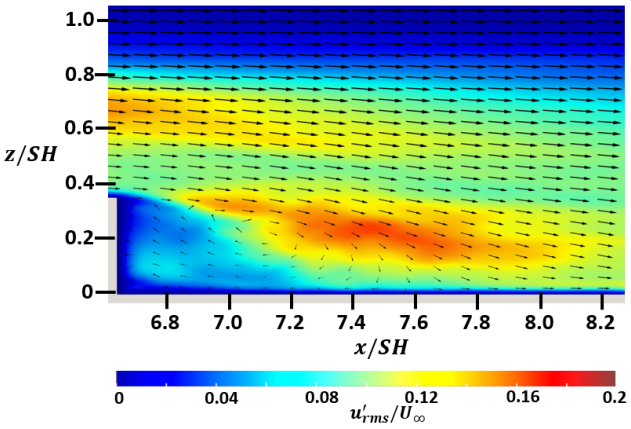

(b) LBM

Figure 14: Streamwise turbulence intensity normalized by the freestream velocity, u'_{rms}/U_∞, obtained from PIV [9] for $Re_L = 3.1 \times 10^6$, and from LBM for $Re_L = 2.9 \times 10^6$, both for uniform inflow conditions at the centerplane of the landing deck.

Figure 14 shows that LBM predicted the streamwise turbulence intensity well. The streamwise turbulence intensity in the freestream was lower compared to the PIV re-

sults. LBM predicted lower turbulence intensities behind the hangar, while PIV results showed moderate turbulence intensity behind the hangar. The high turbulence intensity region was relatively closer to the hangar in the PIV results; on the other hand, the high turbulence intensity region stretched more to the stern in the LBM results. Besides these minor differences, the LBM results correlated well with the PIV results [9], especially for a computationally efficient mid-fidelity approach.

There might be a few reasons behind these differences in turbulence predictions. First, the bounce-back boundary condition applied to the SFS-2 body may have suppressed turbulence formation behind the hangar. Also, the D3Q19 velocity set used for simulations is known to be inferior compared to the D3Q27 set in terms of resolving turbulence. Using the D3Q27 set, which incorporates additional lattice isotropy, might have led to better turbulence results; however, the D3Q27 set requires additional memory resources and leads to additional memory read/write operations during calculations, so the computational performance would be negatively affected.

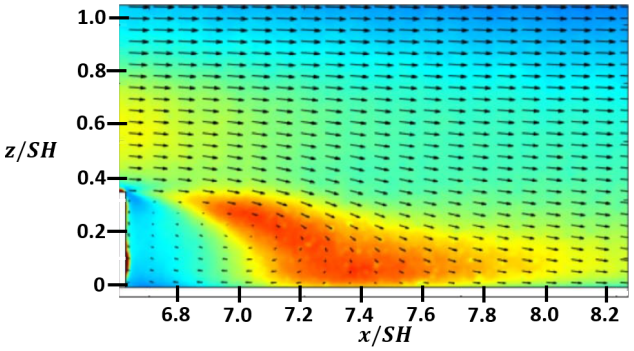

(a) PIV [9]

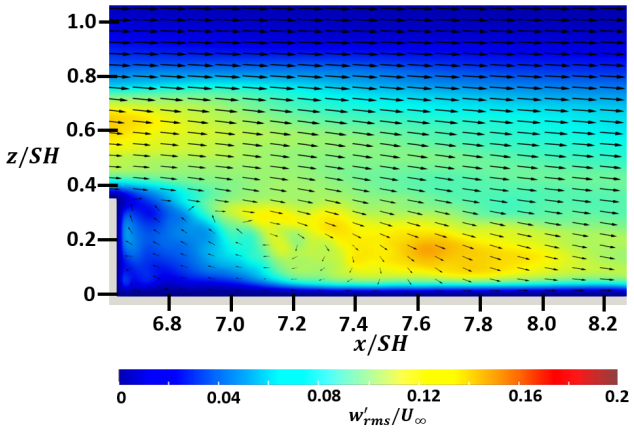

(b) LBM

Figure 15: Vertical turbulence intensity normalized by the freestream velocity, w'_{rms}/U_∞, obtained from PIV [9] for $Re_L = 3.1 \times 10^6$, and from LBM for $Re_L = 2.9 \times 10^6$, both for uniform inflow conditions at the centerplane of the landing deck.

The same observations for the streamwise turbulence intensity can be echoed for the vertical turbulence intensity results shown in Figure 15. Again, LBM predicted a low-turbulence region behind the hangar and high turbulence intensity region farther from the hangar compared to the PIV results [9]. The vertical turbulence intensity was underpredicted by LBM in terms of overall magnitude, although the general behavior/topology correlated well with the PIV results [9].

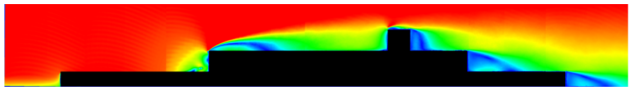

(a) PIV [5]

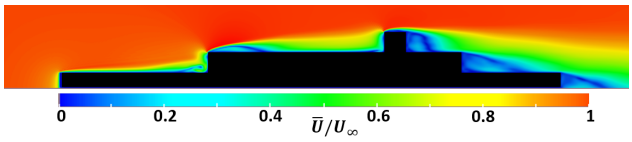

(b) LBM

Figure 16: Time-averaged velocity magnitude normalized by the freestream velocity, $\bar{U}/U_\infty$, PIV results [5] and LBM results both for $Re_L = 2.9 \times 10^6$ in the centerplane for uniform inflow conditions.

In Sydney et al. [5], the centerplane time-averaged velocity magnitude normalized by the freestream velocity was provided for $Re_L = 2.9 \times 10^6$. The PIV measurements were performed for a 1:100 scale SFS-2 model at the same Reynolds number as the LBM calculations. In Figure 16, it can be seen that LBM predicted the flow topology and velocity magnitudes very well over the entire ship centerplane. The separation region behind the funnel was slightly more stretched for the LBM results in comparison to the PIV data. Comparing LBM results with probe data and PIV data by Rosenfeld et al. [4], and with PIV data by Seth et al. [9], it was shown that the current LBM model was able to resolve the flow characteristics on the landing deck accurately. This comparison with the results from Sydney et al. [5] allowed to validate the LBM's consistent accuracy over the entire ship for the mean flow velocities, at least in the centerplane.

CONCLUSIONS

The SFS-2 ship model was simulated with uniform inflow conditions using the Lattice-Boltzmann method (LBM). The obtained results were compared with measurement data from multiple experimental tests using 1:50 scale and 1:100 scale ship models for the same Reynolds number. A convergence study was conducted, yielding a good compromise between physical accuracy of the results and computational expense. The final simulation configuration required three hours and 25 minutes of simulation wall-clock time using eight GPUs on a local GPU cluster, which is only a fraction of the computational expense of more conventional high-fidelity CFD solvers. The results indicated

that the LBM model was well suited for quick estimates on large computational problems, and that it is likely sufficient to be used in piloted ship deck landing flight simulation applications where time-efficient flow field computations are necessary.

From this computational investigation, the following specific conclusions have been drawn:

1. The predicted flow topology and magnitudes obtained for the mean flow field correlated well with the PIV flow field and velocity probe (point) measurements, and sensitivities to exact probe locations were noted.

2. The predicted streamwise turbulence intensity field on the landing deck correlated well with PIV results, except for the recirculation region downstream of the hangar door, where turbulence intensities were underpredicted. The vertical (or wall-normal) turbulence intensity was underpredicted over the entire landing deck up to the hangar height.

3. Using a Cartesian grid and a resolution of $N_{SFS_2} = 700$ computational cells per ship length, convergence in mean and turbulence quantities was obtained. Using the developed LBM model for this flow, the convergent grid resolution cannot be decided by solely monitoring the averaged quantities. Although the simulation with $N_{SFS_2} = 600$ was converged for the mean flow, it was not for the turbulence quantities.

4. Saving much computational expense, an even coarser resolution of $N_{SFS_2} = 400$ produced results that were largely acceptable for the mean flow, except for the region that was very close to the landing deck (i.e., $z/SH < 0.1$) that is less important for a rotorcraft landing approach. Depending on the objectives of a certain simulation, sacrificing some accuracy in the flow field prediction might be a worthwhile trade-off, depending on the desired or needed fidelity levels of the aerodynamic solution (e.g., if used as input into rotorcraft flight dynamics simulations). For $N_{SFS_2} = 700$ the total simulation time was three hours and 25 minutes, for $N_{SFS_2} = 600$ it was one hour and 50 minutes, and for $N_{SFS_2} = 400$ it was less than 50 minutes.

5. The measurements showed an asymmetry between port- and starboard-side flow velocities. While the LBM did not predict this flow asymmetry at the exact probe locations used in the experiments, by slightly shifting the probe locations in the simulations, agreement with the asymmetric experimental data was improved. Additionally, it was seen that certain probe measurements were very sensitive to location, due to their proximity to a strong shear layer. Based on these observations, it was determined that the LBM resolved the major features of the flow field, but may not have exactly predicted the location of the strong shear layer above the landing deck.

6. Using only eight local GPUs, the computational efficiency of the LBM was demonstrated by obtaining results in orders of magnitude less time (three hours and 25 minutes for the converged solution with $N_{SFS_2} = 700$ cells per ship length) than high-fidelity CFD simulations (order of days and weeks on large HPC infrastructure).

ACKNOWLEDGEMENTS

The authors would like to thank the US Navy for supporting this research under grant number N68335-21-C-0336, and specifically Susan Polsky, serving as the technical monitor. Any opinion, findings, and conclusions or recommendations expressed in this material are those of the authors and do not necessarily reflect the views of the United States Government.

CONTACT INFORMATION

All authors are affiliated with the Georgia Institute of Technology in the Daniel Guggenheim School of Aerospace Engineering. Contact emails are listed below.

ekurban3@gatech.edu

sashok@gatech.edu

juergen.rauleder@gatech.edu

REFERENCES

[1] Li, T., Wang, Y., and Zhao, N., "Numerical study of the flow over the modified simple frigate shape," *Journal of Aerospace Engineering*, Vol. 235, (12), September 2021.

[2] Wilkinson, C. H., Zan, S. J., Gilbert, N. E., and Funk, J. D., "Modelling and Simulation of Ship Air Wakes for Helicopter Operations : A Collaborative Venture," RTO Applied Vehicle Technology Panel (AVT) Symposium, Amsterdam, Netherlands, October 5–8, 1998.

[3] Mora, R. B., "Experimental Investigation of the Flow on a Simple Frigate Shape (SFS)," *Scientific World Journal*, Vol. 2014, 2014.

[4] Rosenfeld, N. C., Kimmel, K. R., and Sydney, A. J., "Investigation of Ship Topside Modeling Practices for Wind Tunnel Experiments," 53rd AIAA Aerospace Sciences Meeting, Kissimmee, FL, January 5–9, 2015.

[5] Sydney, A. J., Ramsey, J., and Kimmel, K., "Experimental Investigation of the Turbulent Aerodynamic Environment Produced by a Generic Ship," 54th AIAA Aerospace Sciences Meeting, San Diego, CA, January 4–8, 2016.

[6] Sydney, A. J., Ramsey, J., and Milluzzo, J. I., "Time-Resolved PIV Measurements of Ship Motion and Orientation Effects on Airwake Development," 35th AIAA Applied Aerodynamics Conference, Denver, CO, June 5–9, 2017.

[7] Quon, E. W., Cross, P. A., Smith, M. J., Rosenfeld, N. C., and Whitehouse, G. R., "Investigation of Ship Airwakes Using a Hybrid Computational Methodology," American Helicopter Society 70th Annual Forum, Montréal, QC, May 20–22, 2014.

[8] Farish, D., Seth, D., Thedin, R., and Schmitz, S., "Investigations of ship airwakes using concurrent computations and experiments," Vertical Flight Society Forum 76, Virtual, Online, October 5–8, 2020.

[9] Seth, D., Leishman, J. G., Gnanamanickam, E., and Zhang, Z., "Time-Resolved Ship Airwake Measurements in a Simulated Atmospheric Boundary Layer," *Journal of Aircraft*, Vol. 58, (3), May–June 2021.

[10] Zhu, N., Zhang, Z., Gnanamanickam, E., and Leishman, J. G., "Dynamics of Large-Scale Flow Structures within Ship Airwakes," AIAA Scitech Forum, San Diego, CA, January 3–7, 2022.

[11] Polsky, S. A., "A Computational Study of Unsteady Ship Airwake," 40th AIAA Aerospace Sciences Meeting, Reno, NV, January 14–17, 2002.

[12] Polsky, S. A., "CFD Prediction of Airwake Flowfields for Ships Experiencing Beam Winds," 21st AIAA Applied Aerodynamics Conference, Orlando, FL, June 23–26, 2003.

[13] Polsky, S. A., and Bruner, C. W. S., "A Computational Study of Unsteady Ship Airwake," RTO Applied Vehicle Technology Panel (AVT) Symposium, Loen, Norway, May 7–11, 2001.

[14] Lee, D., Sezer-Uzol, N., Horn, J. F., and Long, L. N., "Simulation of Helicopter Shipboard Launch and Recovery with Time-Accurate Airwakes," *Journal of Aircraft*, Vol. 42, (2), March-April 2005.

[15] Shukla, S., Sinha, S. S., and Singh, S. N., "Ship-Helo Coupled Airwake Aerodynamics: A Comprehensive Review," *Progress in Aerospace Sciences*, Vol. 106, April 2019.

[16] Akcengiz, E. O., and Sezer–Uzol, N., "Ship Airwake Investigations on SFS2 with a Hovering Helicopter Rotor by Computational Fluid Dynamics Simulations," 8th Asian/Australian Rotorcraft Forum, Ankara, Turkey, October 30–November 2, 2019.

[17] Bludau, J., Hajek, M., and Rauleder, J., "Solving the Ship-Rotorcraft Dynamic Interface Problem Using Lattice-Boltzmann Aerodynamics Two-Way Coupled with Blade Element Based Flight Dynamics," Vertical Flight Society Forum 77, Virtual, Online, May 10–14, 2021.

[18] Bludau, J., Rauleder, J., Friedmann, L., and Hajek, M., "Real-Time Simulation of Dynamic Inflow Using Rotorcraft Flight Dynamics Coupled with a Lattice-Boltzmann Based Fluid Simulation," 55th AIAA Aerospace Sciences Meeting, Grapevine, TX, January 9–13, 2017.

[19] Bludau, J., Hajek, M., and Rauleder, J., "Validation of a Dynamic Inflow Model Based on a Flight Dynamics Model and a Lattice–Boltzmann Fluid Solver Using Flight Test Data," 43rd European Rotorcraft Forum, Milan, Italy, September 12–15, 2017.

[20] Horvat, B., Hajek, M., and Rauleder, J., "Computational Flight Path Analysis of a Helicopter in an Offshore Wind Farm Using a Lattice–Boltzmann Method," AIAA Scitech Forum, Virtual, January 11–15 19–21, 2021.

[21] Ashok, S. G., and Rauleder, J., "Investigation of Interpolation Methodologies for Arbitrary Lagrangian Eulerian Lattice–Boltzmann Formulations with Applications to Real–Time Rotorcraft Flight Simulations," AIAA Aviation Forum, Chicago, IL, June 27–July 1, 2022.

[22] Krause, M., Kummerländer, A., Avis, S., Kusumaatmaja, H., Dapelo, D., Klemens, F., Gaedtke, M., Hafen, N., Mink, A., Trunk, R., Marquardt, J., Maier, M., Haussmann, M., and Simonis, S., "OpenLB-Open Source Lattice Boltzmann Code," *Computers and Mathematics with Applications* , Vol. 81, Jan. 2021.

[23] Krüger, T., Kusumaatmaja, H., Kuzmin, A., Shardt, O., Silva, G., and Viggen, E. M., *The Lattice Boltzmann Method: Principles and Practice*, Springer International Publishing, Switzerland, 2017.

[24] Bhatnagar, P. L., Gross, E. P., and Krook, M., "A Model for Collision Processes in Gases. I. Small Amplitude Processes in Charged and Neutral One-Component Systems," *Physical Review*, Vol. 94, (3), May 1954.

[25] Pope, S. B., *Turbulent Flows*, Cambridge University Press, New York, NY, 2000.

[26] Ladd, A. J. C., "Numerical simulations of particulate suspensions via a discretized Boltzmann equation. Part 1. Theoretical foundation," *Journal of Fluid Mechanics*, Vol. 271, 1994.

[27] Blount, D. L., and Bartee, R. J., "Design of Propulsion Systems for High-Speed Craft," *Marine Technology*, Vol. 34, 1997.

[28] Fernandez, I. F., Horvat, B., and Rauleder, J., "Evaluation of Boundary Condition Treatments for Improved Near-Body Solutions in Lattice-Boltzmann Flow Simulations," AIAA Aviation Forum, Chicago, IL, June 27–July 1, 2022.